

Rowan University

Rowan Digital Works

Rowan-Virtua School of Osteopathic Medicine
Faculty Scholarship

Rowan-Virtua School of Osteopathic Medicine

1-2024

Fused In Sarcoma Regulates Glutamate Signaling and Oxidative Stress Response

Chiong-Hee Wong

MacKay Memorial Hospital, Taiwan

Abu Rahat

SUNY - Binghamton

Howard C Chang

Rowan University

Follow this and additional works at: https://rdw.rowan.edu/som_facpub



Part of the [Cell Biology Commons](#), [Disease Modeling Commons](#), [Genetic Processes Commons](#), [Molecular Biology Commons](#), [Molecular Genetics Commons](#), and the [Nervous System Diseases Commons](#)

Recommended Citation

Wong, Chiong-Hee; Rahat, Abu; and Chang, Howard C, "Fused In Sarcoma Regulates Glutamate Signaling and Oxidative Stress Response" (2024). *Rowan-Virtua School of Osteopathic Medicine Faculty Scholarship*. 196.

https://rdw.rowan.edu/som_facpub/196

This Article is brought to you for free and open access by the Rowan-Virtua School of Osteopathic Medicine at Rowan Digital Works. It has been accepted for inclusion in Rowan-Virtua School of Osteopathic Medicine Faculty Scholarship by an authorized administrator of Rowan Digital Works.



Contents lists available at ScienceDirect

Free Radical Biology and Medicine

journal homepage: www.elsevier.com/locate/freeradbiomed

Fused in sarcoma regulates glutamate signaling and oxidative stress response

Chiong-Hee Wong^a, Abu Rahat^b, Howard C. Chang^{c,*}^a Department of Emergency Medicine, MacKay Memorial Hospital, Taipei, 104217, Taiwan^b Integrative Neuroscience Program, SUNY Binghamton, Vestal, NY, 13850, USA^c Department of Cell Biology and Neuroscience, School of Osteopathic Medicine, Rowan University, Stratford, NJ, 08084, USA

A B S T R A C T

Mutations in *fused in sarcoma* (*fust-1*) are linked to ALS. However, how these ALS causative mutations alter physiological processes and lead to the onset of ALS remains largely unknown. By obtaining humanized *fust-1* ALS mutations via CRISPR-CAS9, we generated a *C. elegans* ALS model. Homozygous *fust-1* ALS mutant and *fust-1* deletion animals are viable in *C. elegans*. This allows us to better characterize the molecular mechanisms of *fust-1*-dependent responses. We found FUST-1 plays a role in regulating superoxide dismutase, glutamate signaling, and oxidative stress. FUST-1 suppresses SOD-1 and VGLUT/EAT-4 in the nervous system. FUST-1 also regulates synaptic AMPA-type glutamate receptor GLR-1. We found that *fust-1* ALS mutations act as loss-of-function in SOD-1 and VGLUT/EAT-4 phenotypes, whereas the *fust-1* ALS mutations act as gain-of-function in redox homeostasis and the microbe-induced oxidative stress response. We hypothesized that FUST-1 is a link between glutamate signaling and SOD-1. Our results may provide new insights into the human ALS alleles and their roles in pathological mechanisms that lead to ALS.

1. Introduction

Amyotrophic lateral sclerosis (ALS) is an incurable neurodegenerative disease [1,2]. About 10 % of ALS cases are caused by inheritable mutations [3–7]. Mutations in the ALS genes, including *fused in sarcoma* (*fust-1*), lead to lethality [8–11]. To circumvent this, a classic ALS animal model often contains many copies of a specific human ALS allele in a wild-type background [10,12–14]. Using these overexpression models to delineate the disease mechanism has strengthened the premise that many ALS mutations are gain-of-function [15]. However, the lack of a suitable single-copy endogenous ALS model has limited our ability to fully understand the mechanism of ALS pathology.

One of the hallmarks of ALS disease is the aberrant accumulation of SOD-1 [16,17]. SOD-1 is an enzyme that converts superoxide into less-toxic hydrogen peroxide and oxygen [18–20]. It has been recently hypothesized that many ALS genes may play a concerted role in regulating a specific set of physiological and pathological processes [3]. For example, the accumulation of SOD-1 in motor neurons caused by mutations in other ALS causative genes may be a common pre-clinical phenotype that leads to ALS.

As evidenced by the protective effect of the glutamatergic neurotransmission blocker riluzole in ALS patients [21,22], another pathological process associated with ALS is an increase in glutamate signaling

[23,24]. In *C. elegans*, *eat-4* encodes a mammalian homolog of glutamate vesicular transporter VGLUT [25,26] and *glr-1* encodes a mammalian homolog of AMPA-type glutamate receptor subunit GluR1 [27,28]. The molecular mechanism of *fust-1*-dependent regulation of EAT-4 and GLR-1 currently remains largely unknown.

It has been hypothesized that elevation of oxidative stress may contribute to ALS [13,29]. Recent work has shown that exposing nematodes to pathogens *P. aeruginosa* PA14 causes elevation of reactive oxygen species (ROS) and an increase in SOD-1 expression [30,31]. In addition, both *eat-4* and *glr-1* mutations elicited an altered behavioral response to *P. aeruginosa* PA14 [32]. This prompts us to use this host–pathogens paradigm to delineate *fust-1* ALS mutants with regard to their sensitivity to oxidative stress.

We hypothesized that FUST-1 regulates SOD-1 and glutamate signaling. To test this hypothesis, we first obtained *fust-1* ALS alleles *fust-1* (R446S) and *fust-1*(P447L) in *C. elegans*. Mutations of *fust-1* (R446S) and *fust-1*(P447L) correspond to human *fused in sarcoma* (R524S) and (P525L) alleles, respectively [33]. Because of a mutation in the nuclear localization sequence, human FUST-1 (R524S) and FUST-1 (P525L) proteins are mislocalized in the cytoplasm and are present in stress granules [34–38]. Unlike other animal models, homozygous *fust-1* ALS mutant and homozygous *fust-1* deletion nematodes are viable under laboratory growing conditions [33]. This allows us to tackle questions

* Corresponding author.

E-mail address: changh@rowan.edu (H.C. Chang).<https://doi.org/10.1016/j.freeradbiomed.2023.11.015>

Received 7 July 2023; Received in revised form 21 September 2023; Accepted 16 November 2023

Available online 23 November 2023

0891-5849/© 2023 The Authors. Published by Elsevier Inc. This is an open access article under the CC BY-NC-ND license (<http://creativecommons.org/licenses/by-nc-nd/4.0/>).

that are difficult to address, such as the genetic nature of an ALS allele in distinct physiological processes.

In this study, we examined the role of FUST-1 in motor neuron-specific regulation of SOD-1. We also investigated the EAT-4 and GLR-1 phenotypes of *fust-1* deletion and *fust-1* ALS mutant alleles. Finally, we generated a redox reporter and measured the ROS in *fust-1* mutations with or without oxidative stress triggered by *P. aeruginosa* PA14. We found that *fust-1* (R446S) and *fust-1* (P447L) act as loss-of-function mutations in the context of SOD-1 and EAT-4 regulation. FUST-1 suppresses SOD-1 elevation in cholinergic motor neurons. FUST-1 also suppresses excess EAT-4 in the nervous system. In contrast, we found that *fust-1* (R446S) and *fust-1* (P447L) act as gain-of-function mutations in the ROS response. The unexpected differences regarding the nature of *fust-1* ALS mutations in the ROS response and glutamate signaling illustrate the significance of using single-copy endogenous mutations to model a human disease such as ALS.

2. Results

2.1. FUST-1 is expressed ubiquitously and is present in cholinergic motor neurons in *C. elegans*

We began our study by obtaining a deletion and two point mutations of *fust-1*, namely *fust-1* (*tm4439*), *fust-1* (R446S), and *fust-1* (P447L), respectively (Fig. 1A). To mimic human ALS mutations *fust-1* (R524S) and *fust-1* (P525L), *fust-1* (R446S) and *fust-1* (P447L) were generated by modifying the corresponding loci of *fust-1* in *C. elegans*. To assess the FUST-1 expression of these *fust-1* mutations, we generated a polyclonal antibody against the carboxyl region of FUST-1. We then performed immunohistochemistry analysis using crude worm lysates. We found a single band of ~46 kD (predicted molecular weight of FUST-1) in wild-type, *fust-1* (R446S), and *fust-1* (P447L). In contrast, the band is absent in *fust-1* (*tm4439*) deletion (Fig. 1B). Therefore, we reasoned that *fust-1* (*tm4439*) is likely acting as a null. We then generated a *fust-1p*:FUST-1mStrawberry transgene and introduced it into the *fust-1* (*tm4439*) background. We found a single band of ~74 kD representing the FUST-1mStrawberry fusion protein (Fig. 1B). We blotted the same membrane

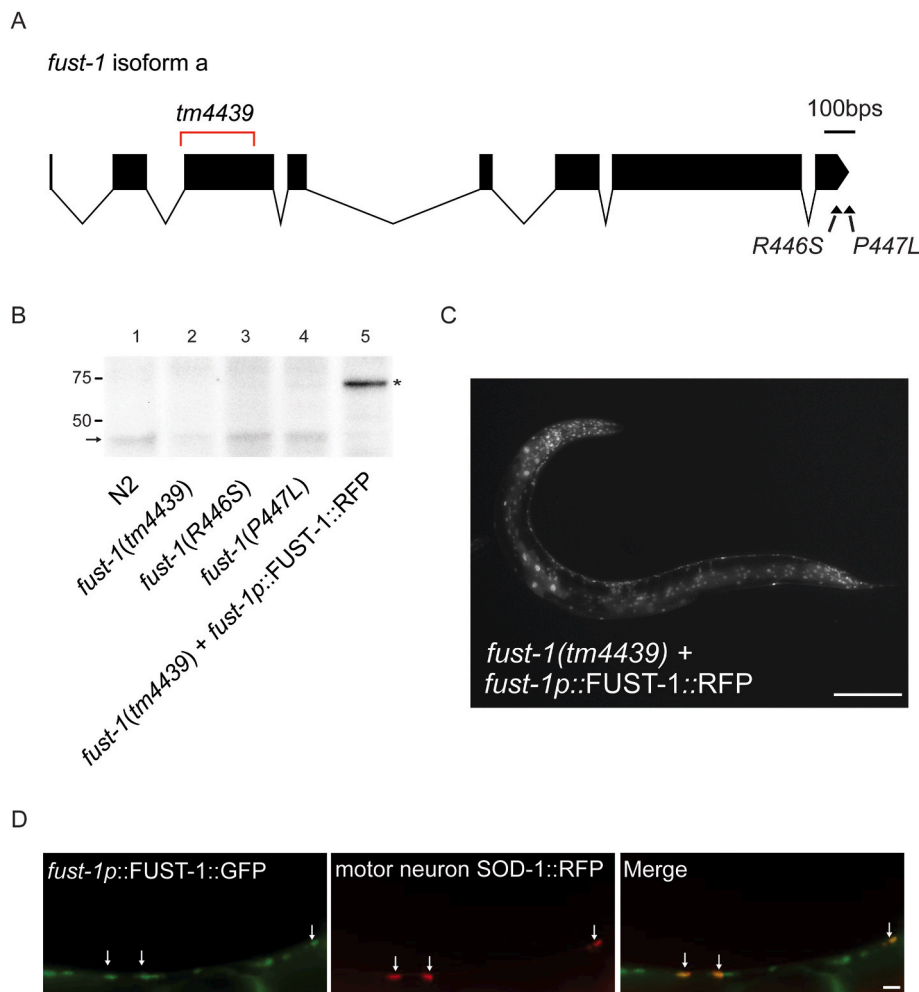


Fig. 1. FUST-1 is expressed in cholinergic motor neurons in *C. elegans*.

(A) Scheme of the *fust-1* genomic region. The deleted region in *fust-1* (*tm4439*) is indicated in red. The point mutations of *fust-1* (R446S) and *fust-1* (P447L) are indicated with arrows. Black boxes indicate exons. Connected lines indicate the region of an intron.

(B) FUST-1 immunohistochemistry results using lysates derived from wild-type N2, *fust-1* (*tm4439*), *fust-1* (R446S), *fust-1* (P447L), and *fust-1* (*tm4439*); *fust-1p*:FUST-1mStrawberry transgenic worms. Arrow represents the size of wild-type FUST-1. Star represents the FUST-1mStrawberry fusion protein.

(C) Fluorescence micrographs of *fust-1p*:FUST-1mStrawberry in *fust-1* (*tm4439*) background. mStrawberry signals are present ubiquitously and are localized predominantly in the nucleus. Scale bar indicates 150 μ m.

(D) Fluorescence micrographs of *fust-1p*:FUST-1GFP (left), *unc129p*:SOD-1mScarlet (middle), and the merge of the two (right). Arrows indicate DA- and DB-type cholinergic motor neurons. Scale bar indicates 10 μ m.

with antibody against β -tubulin. We found *fust-1* (*tm4439*) deletion has a reduced level of β -tubulin. The reduction of β -tubulin in *fust-1* (*tm4439*) deletion can be rescued by *fust-1p:FUST-1mStrawberry* (Supplemental Fig. 1). As indicated by the fluorescence image of *fust-1p:FUST-1mStrawberry*, FUST-1 is localized in the nucleus and is present ubiquitously in many tissues, including the nervous system and intestine (Fig. 1C). Finally, we used *unc-129p:SOD-1mScarlet* as a co-localization marker to determine whether FUST-1 is expressed in motor neurons. As *unc-129* promoter confers SOD-1mScarlet expression in DA and DB motor neurons at the ventral nerve cord. We introduced *unc-129p:SOD-1mScarlet* and *fust-1p:FUST-1GFP* into the same background. We found that FUST-1GFP partially co-localized with SOD-1mScarlet (Fig. 1D). This result suggests that FUST-1 is present in the cholinergic motor neurons in *C. elegans*.

2.2. SOD-1 expression is suppressed by FUST-1 in cholinergic motor neurons

To investigate the role of FUST-1 in SOD-1 regulation, we first introduced *unc-129p:SOD-1mScarlet* into *fust-1* (*tm4439*). We found the fluorescence intensity of SOD-1mScarlet is elevated in DA and DB motor neurons (Supplemental Fig. 2). We decided to measure the fluorescence intensity of DA7 as a representation of the SOD-1mScarlet increase in motor neurons. After we introduced a *fust-1* genomic rescue fragment into *fust-1* (*tm4439*), this increase of SOD-1mScarlet in DA7 motor neuron was restored to the wild-type level (Fig. 2A). We then introduced *unc-129p:SOD-1mScarlet* into *sod-1*; *fust-1* double mutants and found a similar increase in SOD-1mScarlet intensity in DA7 motor neuron (Fig. 2C). This suggests the increase of SOD-1mScarlet in *fust-1* single mutants (Fig. 2A) is likely not due to the unintended effect of SOD-1 overexpression in a SOD-1 wild-type background. We found that SOD-1mScarlet is also elevated in DA7 of *fust-1* (*R446S*) and *fust-1*(*P447L*)

(Fig. 2B). Compared to *fust-1* (*tm4439*) deletion, the increase of SOD-1mScarlet in *fust-1* (*R446S*) and *fust-1*(*P447L*) is to a lesser extent (Fig. 2A and B). These results suggest that ALS *fust-1* (*R446S*) and *fust-1* (*P447L*) are acting as hypomorphic mutations of *fust-1* in the context of motor neuron-specific regulation of SOD-1. The aforementioned results also suggest that FUST-1 suppresses the elevation of SOD-1.

2.3. Loss of *fust-1* causes an increase in glutamate transporter in the nervous system

Glutamate transporter EAT-4 is the *C. elegans* homolog of mammalian VGLUT [25,26]. Synaptic EAT-4GFP is localized at the ventral nerve cord as punctate structures [32]. To investigate the role of FUST-1 in glutamate signaling, we introduced EAT-4GFP into *sod-1* (*tm776*), *fust-1* (*R446S*), *fust-1*(*P447L*), and *fust-1* (*tm4439*) (Fig. 3A). We found that the intensity of EAT-4GFP is not altered in *sod-1* (*tm776*). In contrast, *fust-1* (*tm4439*) animals showed a strong increase in EAT-4GFP intensity compared to wild-type (Fig. 3B). ALS mutants *fust-1* (*R446S*) and *fust-1* (*P447L*) also showed an increase in EAT-4GFP intensity, but to a lesser extent compared to *fust-1* (*tm4439*) (Fig. 3B). The increase of EAT-4GFP intensity in *fust-1* (*tm4439*) deletion, *fust-1* (*R446S*), and *fust-1*(*P447L*) is rescued by a genomic fragment of *fust-1* (Supplemental Fig. 3). These results suggest that FUST-1 plays a role in regulating glutamate transporter EAT-4 at the synapses. In addition, *fust-1* (*R446S*) and *fust-1* (*P447L*) are acting as hypomorphic mutations of *fust-1* in the EAT-4-dependent phenotype.

2.4. FUST-1 modulates AMPA-type ionotropic glutamate receptor GLR-1

Since FUST-1 suppresses EAT-4 at the ventral nerve cord, we sought to determine whether FUST-1 regulates synaptic AMPA-type ionotropic glutamate receptor GLR-1. GLR-1 is the mammalian homolog of GluR1

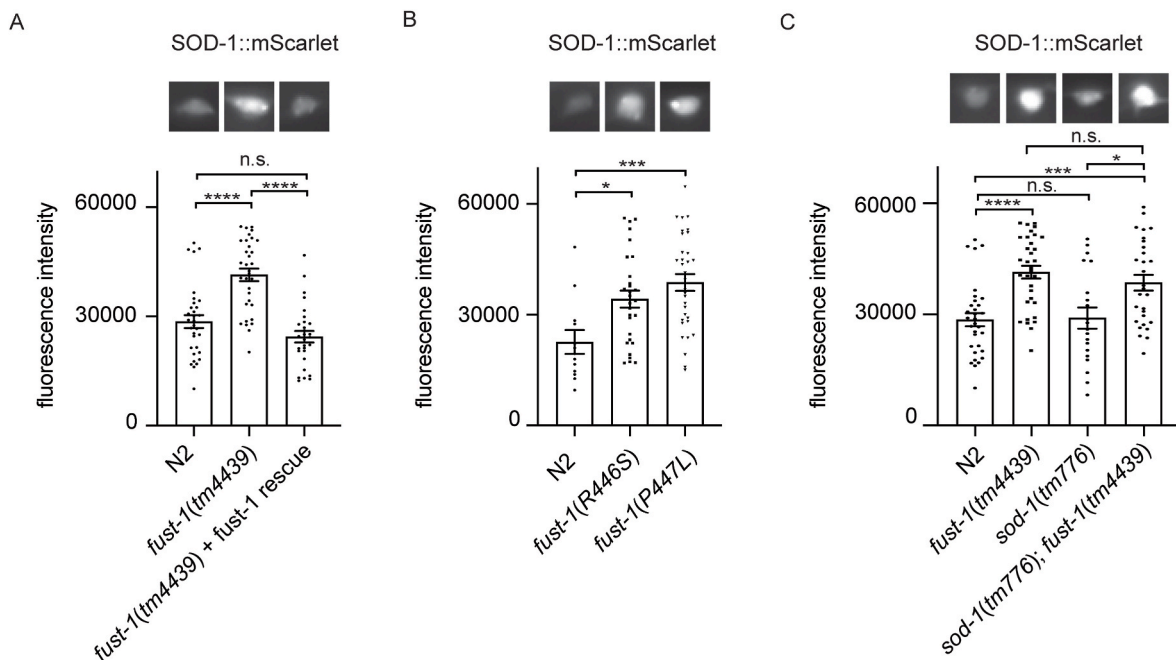


Fig. 2. FUST-1 suppresses excess SOD-1 in motor neurons.

(A) Motor neuron-specific SOD-1 expression is elevated in *fust-1* (*tm4439*) background. By introducing a genomic fragment that contains *fust-1*, the fluorescence intensity of SOD-1mScarlet in *fust-1* (*tm4439*) is restored to a level similar to wild-type. Error bar represents s. e.m. **** represents $p < 0.0001$. Ns represents not significant. As determined by one-way ANOVA, followed by Tukey's multiple comparison analysis. $N \geq 29$.

(B) Motor neuron-specific SOD-1 expression is elevated in *fust-1* (*R446S*) and *fust-1*(*P447L*). Error bar represents s. e.m. * represents $p < 0.05$. *** represents $p < 0.001$. Ns represents not significant. As determined by one-way ANOVA, followed by Tukey's multiple comparison analysis. $N \geq 15$.

(C) Motor neuron-specific SOD-1 expression in *sod-1* (*tm776*); *fust-1* (*tm4439*) double mutant is similar to *fust-1* (*tm4439*) single mutant. Error bar represents s. e.m. **** represents $p < 0.0001$. **** represents $p < 0.0001$. Ns represents not significant. As determined by one-way ANOVA, followed by Tukey's multiple comparison analysis. $N \geq 20$.

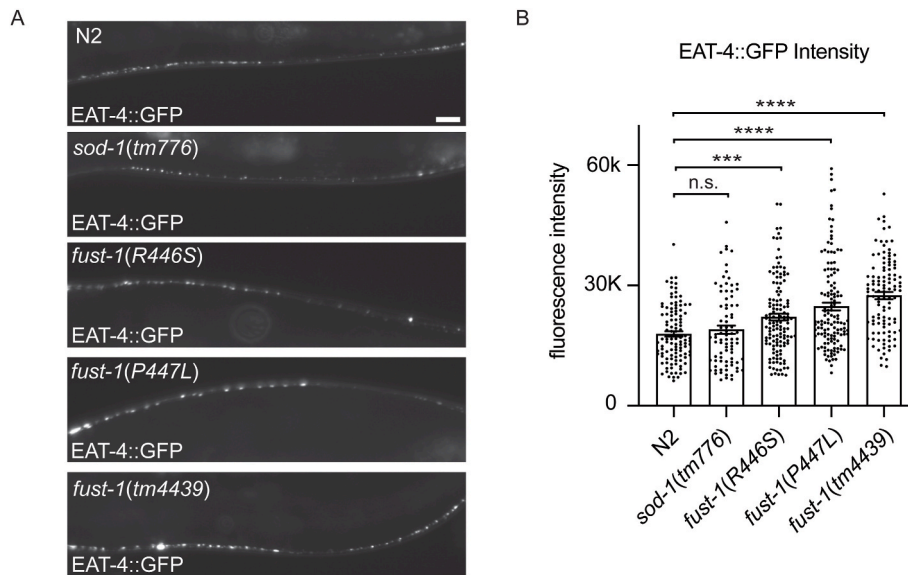


Fig. 3. FUST-1 regulates glutamate transporter EAT-4 at the ventral nerve cord. (A) Representative fluorescence micrographs of *eat-4p*:EAT-4GFP in wild-type N2, *sod-1* (*tm776*), *fust-1* (*R446S*), *fust-1* (*P447L*), and *fust-1* (*tm4439*) backgrounds. Scale bar indicates 10 μ m. (B) *fust-1* (*tm4439*) shows the strongest increase in EAT-4GFP intensity. *fust-1* (*R446S*) and *fust-1* (*P447L*) show an intermediate increase in EAT-4GFP intensity. Error bar represents s. e.m. *** represents $p < 0.001$. **** represents $p < 0.0001$. Ns represents not significant. As determined by one-way ANOVA, followed by Tukey's multiple comparison analysis. $N \geq 20$.

in *C. elegans* [39,40] and is localized as punctate structures at the ventral nerve cord [27,41]. We introduced GLR-1GFP into *fust-1* (*tm4439*), *fust-1* (*R446S*), and *fust-1* (*P447L*) (Fig. 4A). We found that the density of GLR-1GFP at the ventral nerve cord is increased in all *fust-1* mutations. In addition, the size of synaptic GLR-1GFP is reduced in all *fust-1* mutations (Fig. 4B and C). Compared to wild-type, the intensity of GLR-1GFP is reduced in *fust-1* (*tm4439*). In contrast, the intensity of GLR-1GFP is increased in *fust-1* (*R446S*) and *fust-1* (*P447L*) (Fig. 4D). These results suggest that FUST-1 modulates AMPA-type ionotropic glutamate receptor GLR-1 at the ventral nerve cord.

2.5. Gut oxidative homeostasis is altered in *fust-1* mutations

To investigate the role of FUST-1 in oxidative stress, we generated a transgene that confers expression of a redox fluorescence reporter rxRFP [42] in the nervous system and intestine. Due to undetectable baseline expression of rxRFP in the nervous system, we decided to focus our analyses on the intestine. We introduced the rxRFP reporter into *fust-1* (*tm4439*), *fust-1* (*R446S*), and *fust-1* (*P447L*) and measured rxRFP fluorescence intensity (Fig. 5A). We found the intensity of rxRFP is higher in *fust-1* (*R446S*) and *fust-1* (*P447L*) (Fig. 5B). Compared to wild-type, the intensity of rxRFP is lower in *fust-1* (*tm4439*) (Fig. 5C and D). The reduction in rxRFP intensity in *fust-1* (*tm4439*) can be restored by a *fust-1* genomic fragment (Fig. 5C and D). In addition, heterozygous *fust-1* (*R446S*)/+ and *fust-1* (*P447L*)/+ animals showed a stronger rxRFP fluorescence intensity compared to +/+ animals (Supplemental Fig. 4). These data indicate *fust-1* (*R446S*) and *fust-1* (*P447L*) animals have the opposite phenotype in ROS homeostasis to *fust-1* (*tm4439*). Our data suggest *fust-1* (*R446S*) and *fust-1* (*P447L*) are gain-of-function mutations in ROS response. Together, these results suggest FUST-1 plays a role in regulating oxidative homeostasis.

2.6. FUST-1 ALS mutants elicit a heightened response to oxidative stress triggered by *P. Aeruginosa* PA14

Exposure to *P. aeruginosa* PA14 causes an increase in oxidative stress in *C. elegans* [30]. To investigate the role of FUST-1 in the pathogen-induced ROS response, we transferred the rxRFP containing

wild-type and *fust-1* mutant animals onto a Petri dish with a lawn of *P. aeruginosa* PA14 and recorded the rxRFP fluorescence after 8 h. Similar to previous observations [30], wild-type animals showed an increase in ROS after 8 h exposure to *P. aeruginosa*, as indicated by an increase in gut rxRFP fluorescence (Fig. 6A and B). The ROS in *fust-1* deletion showed a similar increase after 8 h (Fig. 6A and B). Without *P. aeruginosa* exposure, *fust-1* (*R446S*) and *fust-1* (*P447L*) animals elicited a higher baseline of ROS (Fig. 5A and B). After 8 h exposure to *P. aeruginosa*, the *fust-1* (*R446S*) and *fust-1* (*P447L*) animals elicited a further increase in ROS (Fig. 6C and D). This indicates that *fust-1* ALS mutant animals have a higher sensitivity to *P. aeruginosa*-induced oxidative stress.

2.7. FUST-1 ALS alleles contribute to heightened pathogen avoidance response

Elevation in pathogen-induced oxidative stress is often associated with pathogen avoidance behavior [30,31]. Therefore, we sought to investigate the role of FUST-1 in *C. elegans* behavioral response to pathogens. We performed the pathogen avoidance assay by transferring *fust-1* (*tm4439*), *fust-1* (*R446S*), and *fust-1* (*P447L*) animals onto a Petri dish that contained a small lawn of *P. aeruginosa* PA14 [43]. After 7 h, *fust-1* (*R446S*) and *fust-1* (*P447L*) animals showed a heightened pathogen avoidance response compared to wild-type (Fig. 7A). In contrast, *fust-1* (*tm4439*) deletion showed an avoidance response similar to wild-type (Fig. 7B). By overexpressing a *fust-1* transgene in *fust-1* (*tm4439*), the aforementioned animals showed a heightened avoidance to *P. aeruginosa* (Fig. 7B). Together, these results suggest *fust-1* (*R446S*) and *fust-1* (*P447L*) are acting as gain-of-function alleles in behavioral and oxidative stress response to pathogens.

Here, we showed that FUST-1 is present in cholinergic motor neurons in *C. elegans*. In motor neurons, FUST-1 suppresses SOD-1 elevation. FUST-1 also suppresses excess EAT-4 in the nervous system. In addition, a lack of FUST-1 increases the density of synaptic GLR-1. Our data suggest that *fust-1* ALS alleles are loss-of-function mutations in SOD-1 and EAT-4 phenotypes. When grown on *E. coli*, *fust-1* deletion animals elicited a reduction in ROS, whereas *fust-1* ALS mutants elicited an increase in ROS. Finally, *fust-1* ALS mutants showed a heightened

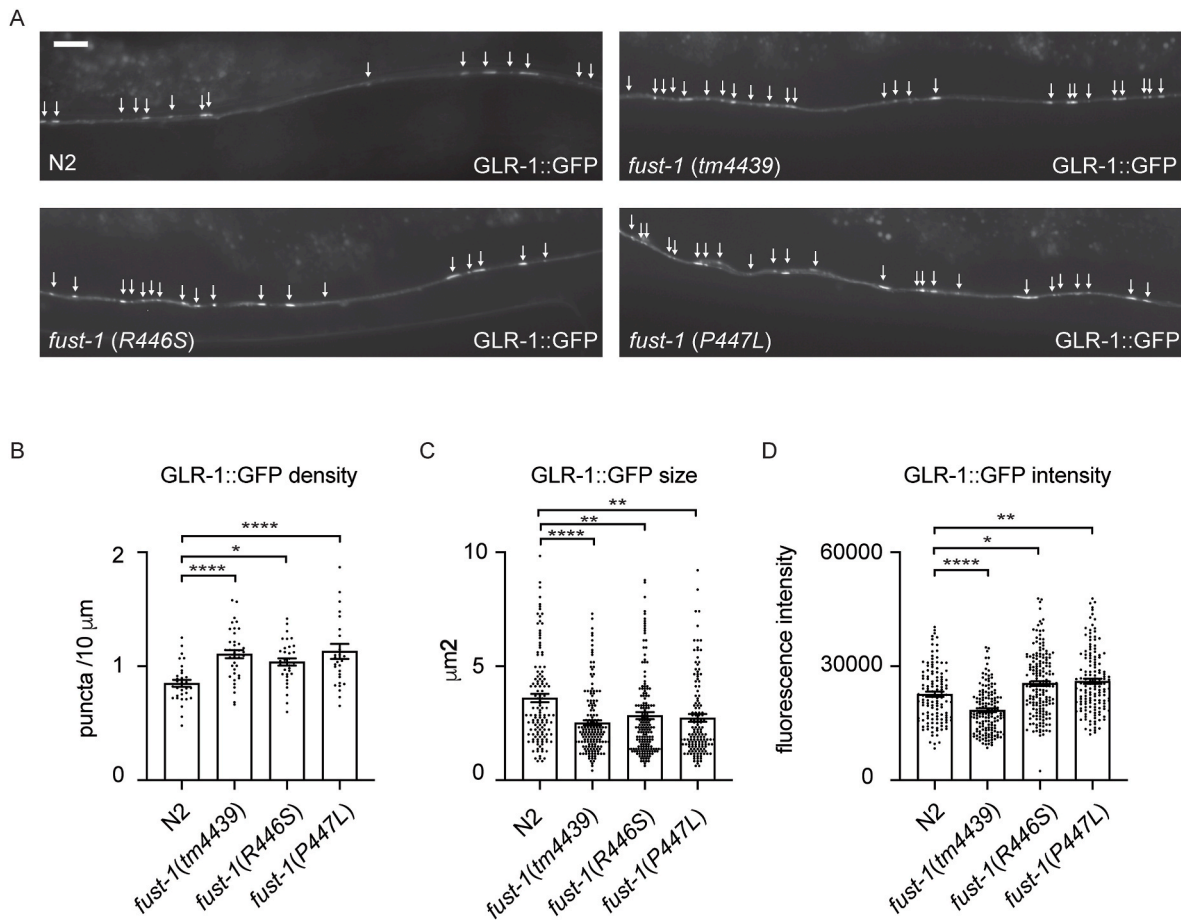


Fig. 4. FUST-1 plays a role in regulating synaptic GLR-1 at the ventral nerve cord.

(A) Fluorescence micrographs of *glr-1p::GLR-1::GFP* in wild-type N2, *fust-1(tm4439)*, *fust-1(R446S)*, and *fust-1(P447L)*. Arrow indicates GLR-1::GFP. Scale bar indicates 10 μm .

(B) *fust-1(tm4439)*, *fust-1(R446S)*, and *fust-1(P447L)* mutant animals show an increase in GLR-1::GFP density compared to wild-type.

(C) *fust-1(tm4439)*, *fust-1(R446S)*, and *fust-1(P447L)* mutant animals elicit a reduced GLR-1::GFP size.

(D) *fust-1(R446S)* and *fust-1(P447L)* mutant animals show an increase in GLR-1::GFP fluorescence intensity. Compared to wild-type, a reduced GLR-1::GFP intensity was observed in *fust-1(tm4439)*.

(B–D) Error bar represents s. e. m. * represents $p < 0.05$. ** represents $p < 0.01$. **** represents $p < 0.0001$. Ns represents not significant. As determined by one-way ANOVA, followed by Tukey's multiple comparison analysis. $N \geq 18$.

sensitivity in pathogen-induced oxidative stress and behavioral response. Our results suggest that *fust-1* ALS alleles are gain-of-function mutations in redox homeostasis and the microbe-induced stress response. The loss-of-function vs. gain-of-function differences of *fust-1* ALS alleles in distinct physiological processes demonstrate the importance of using single-copy endogenous mutations to model ALS.

3. Discussion

Research to define the pathological processes of amyotrophic lateral sclerosis has facilitated therapeutics development. It includes drugs to alleviate oxidative stress, reduce glutamate excitotoxicity, and maintain ER and mitochondrial homeostasis [22,44–46]. However, a cure for this fetal neurodegenerative disease is not yet achievable with either one of or with the combination of these medications. This illustrates the need to identify additional disease mechanisms that lead to the malaise of ALS.

To create a nematode ALS model, ALS mutations were obtained by modifying the endogenous loci of *fust-1* via CRISPR-CAS9 (Fig. 1) [32, 47–49]. These homozygous ALS mutant nematodes are viable [32,33]. In addition, these ALS worms showed changes in neurophysiology similar to what was found in ALS patients (Figs. 2 and 3). Thus, the single-copy ALS model has opened a door for us to investigate the role of

FUST-1 in distinct physiological processes that contribute to the pathology in the nervous system.

Compared to *fust-1* deletion, *fust-1(R446S)* and *fust-1(P447L)* animals elicited an increase in EAT-4 and SOD-1, but to a lesser extent (Figs. 2 and 3). Based on previous studies [10,14], we originally thought that *fust-1(R446S)* and *fust-1(P447L)* were gain-of-function. Instead, we discovered that *fust-1(R446S)* and *fust-1(P447L)* are hypomorphic mutations of *fust-1* in the context of EAT-4 and SOD-1 regulation. Due to a lack of deletion/null mutation as a control in an overexpression ALS model, we reasoned this may contribute to the differences in interpretation regarding the nature of *fust-1* ALS mutations.

In contrast, we found that *fust-1(R446S)* and *fust-1(P447L)* act as gain-of-function mutations in the ROS response. The ROS reporter rxRFP intensity was elevated in the intestine of *fust-1(R446S)* and *fust-1(P447L)* when they were on an *E. coli* diet. In contrast, the ROS reporter rxRFP intensity was reduced in *fust-1(tm4439)* deletion (Fig. 5). In addition, *fust-1(R446S)* and *fust-1(P447L)* animals elicited a more robust response to pathogen-induced oxidative stress (Fig. 6). A heightened avoidance response to *P. aeruginosa* was also observed in *fust-1(R446S)* and *fust-1(P447L)* (Fig. 7).

Due to an undetectable baseline expression of rxRFP in the nervous system, in this report, we focused on investigating the changes of ROS in

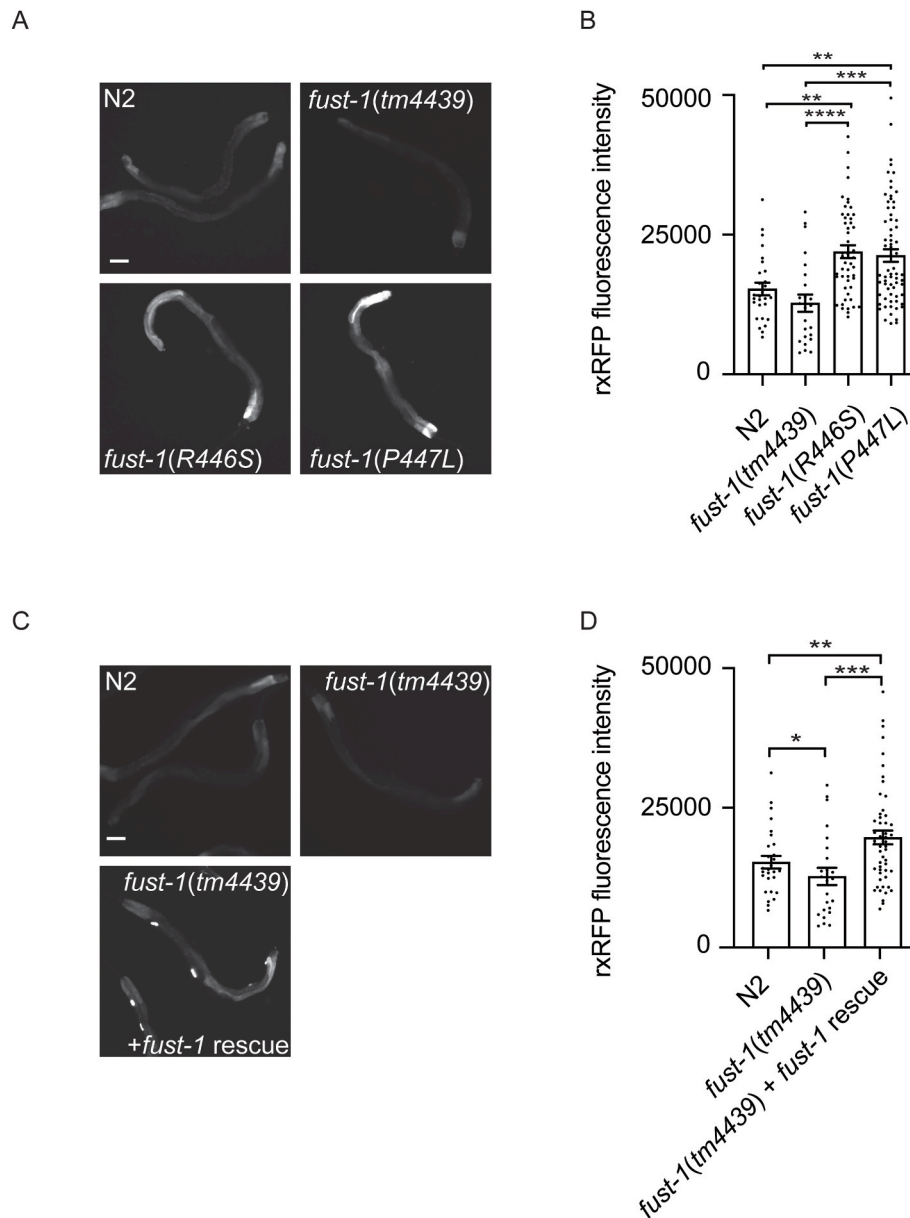


Fig. 5. FUST-1 modulates reactive oxygen species levels in the intestine.

(A) Fluorescence micrographs of redox reporter rxRFP in wild-type N2, *fust-1* (*tm4439*), *fust-1* (*R446S*), and *fust-1* (*P447L*). Scale bar indicates 150 μ m

(B) The gut rxRFP fluorescence is increased in *fust-1* (*R446S*) and *fust-1* (*P447L*). Error bar represents s. e.m. ** represents $p < 0.01$. *** represents $p < 0.001$. **** represents $p < 0.0001$. As determined by one-way ANOVA, followed by Tukey's multiple comparison analysis. $N \geq 24$.

(C) Fluorescence micrographs of redox reporter rxRFP in wild-type N2, *fust-1* (*tm4439*), and *fust-1* (*tm4439*) + *fust-1* rescue. Scale bar indicates 150 μ m.

(D) The gut rxRFP fluorescence is reduced in *fust-1* (*tm4439*). By introducing a *fust-1* fragment into *fust-1* (*tm4439*), the rxRFP intensity is increased. Error bar represents s. e.m. * represents $p < 0.05$. ** represents $p < 0.01$. *** represents $p < 0.001$. It is determined by Student's *t*-test. $N \geq 24$. (A–D) All animals were grown on petri dishes containing staple food *E. coli* OP50.

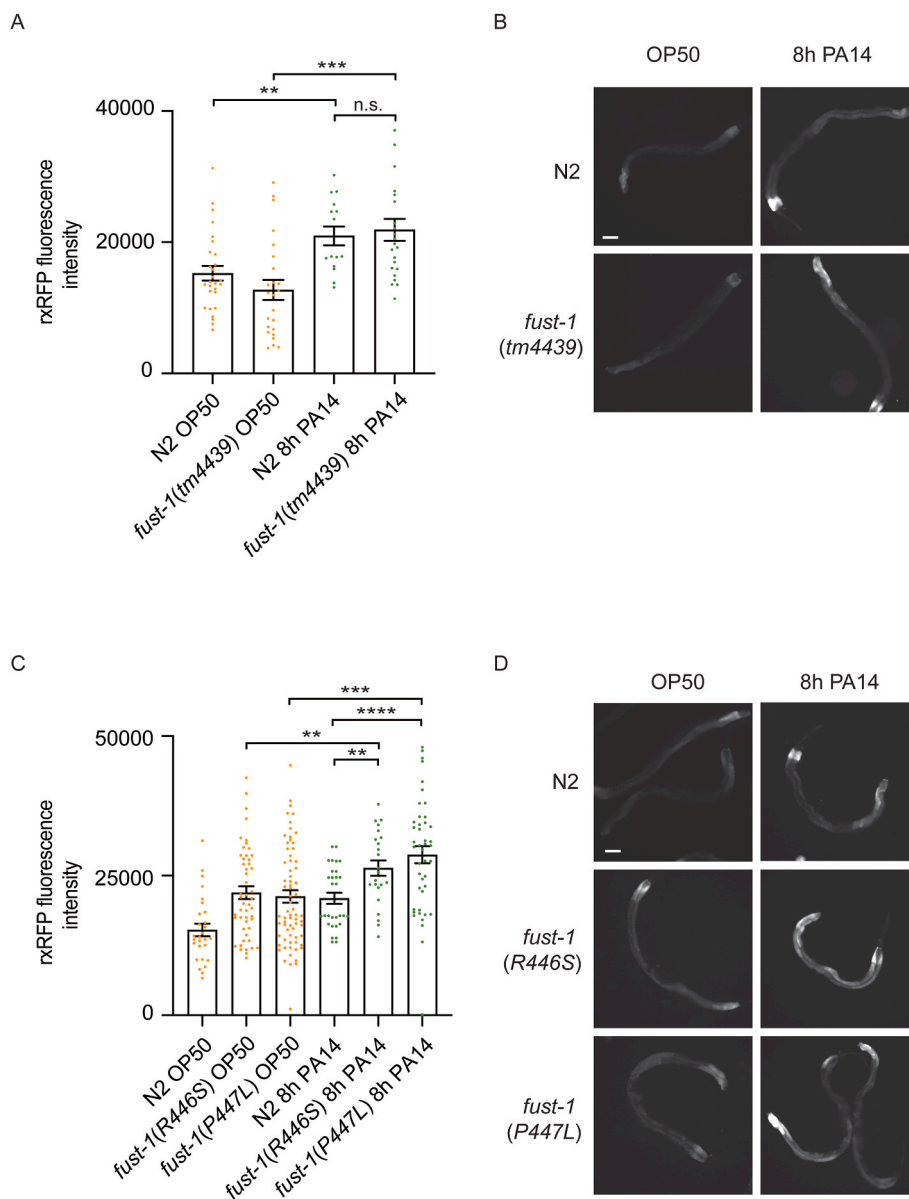


Fig. 6. FUST-1 ALS mutant animals elicit an increase in ROS after exposure to *P. aeruginosa* PA14.

(A) Fluorescence intensity of intestinal rxRFP in wild-type and *fust-1* (*tm4439*). Animals were on *E. coli* OP50 or switched to *P. aeruginosa* PA14 for 8 h. A similar increase in rxRFP intensity was observed in wild-type and *fust-1* (*tm4439*) animals after 8 h. Error bar represents s. e.m. ** represents $p < 0.01$. *** represents $p < 0.001$. Ns represents not significant. As determined by one-way ANOVA, followed by Tukey's multiple comparison analysis. $N \geq 17$.

(B) Fluorescence micrographs illustrating the intestinal rxRFP of wild-type and *fust-1* (*tm4439*) on *E. coli* OP50 or 8 h on *P. aeruginosa* PA14.

(C) Fluorescence intensity of intestinal rxRFP in *fust-1* (*R446S*) and *fust-1* (*P447L*). Animals were on *E. coli* OP50 or switched to *P. aeruginosa* PA14 for 8 h. A further increase in rxRFP intensity was observed in *fust-1* (*R446S*) and *fust-1* (*P447L*) after 8 h. Error bar represents s. e.m. ** represents $p < 0.01$. *** represents $p < 0.001$. **** represents $p < 0.0001$. As determined by Student's *t*-test. $N \geq 20$.

(D) Fluorescence micrographs illustrating the intestinal rxRFP of wild-type, *fust-1* (*R446S*), and *fust-1* (*P447L*) animals on *E. coli* OP50 or 8 h on *P. aeruginosa* PA14.

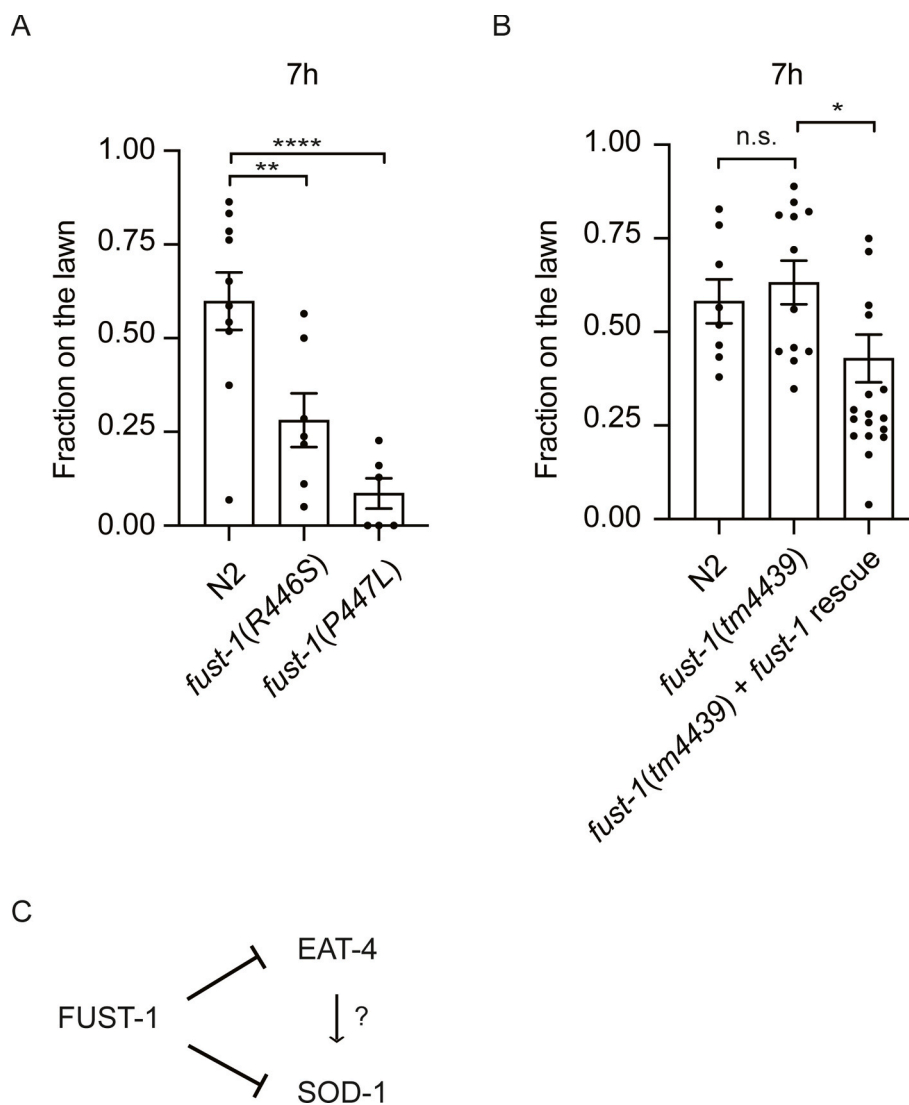


Fig. 7. FUST-1 ALS mutant animals elicit a heightened pathogen avoidance response.

(A) Pathogen avoidance response of *fust-1 (R446S)* and *fust-1(P447L)* at 7 h.

Error bar represents s. e.m. ** represents $p < 0.01$. **** represents $p < 0.0001$. As determined by Student's *t*-test. $N \geq 9$.

(B) Pathogen avoidance response of *fust-1 (tm4439)* at 7 h. Overexpressing *fust-1* in *fust-1 (tm4439)* enhances the avoidance response.

Error bar represents s. e.m. * represents $p < 0.05$. Ns represents not significant. As determined by Student's *t*-test. $N \geq 9$

(C) Working hypothesis of FUST-1-dependent regulation of EAT-4 and SOD-1 in the nervous system.

the intestine. Since the intestine is where *P. aeruginosa* accumulate, we reasoned that the gut rxRFP is a reasonable reporter to delineate the ROS levels of a *fust-1* mutant. Future studies using a strong motor neuron-specific promoter to drive rxRFP expression may better illustrate the neuron-specific ROS response regulated by FUST-1.

Excitatory glutamatergic transmission plays a key role in mediating oxidative stress [50,51]. Indeed, both *fust-1* (R446S) and *fust-1*(P447L) mutants showed an increase in the intensity and density of GLR-1GFP at the ventral nerve cord (Fig. 4). These results correlate with the increase of ROS observed in *fust-1* (R446S) and *fust-1*(P447L) (Fig. 5). In *fust-1* (tm4439) deletion, the overall GLR-1GFP intensity is reduced (Fig. 4D). The reduction of GLR-1GFP intensity may offer a possible explanation regarding the reduction of ROS in *fust-1* (tm4439) (Fig. 5D). It remains to be tested whether aberrant cytoplasmic localization of FUST-1 (R446S) and FUST-1(P447L) in stress granules contributes to the increase of ROS.

The data presented here establish that FUST-1 plays a role in regulating SOD-1, EAT-4, and GLR-1. We hypothesize that FUST-1 may be the link between the SOD-1-dependent response and glutamate signaling in the nervous system (Fig. 7C and graphical abstract). In contrast to *fust-1* deletion, *fust-1* ALS alleles cause elevation of ROS. These results may provide insights into the pathological processes that lead to ALS and potential targets for ALS treatments.

4. Material and methods

4.1. Resource availability

4.1.1. Lead contact

Further information and requests for resources and reagents should be directed to and will be fulfilled by the lead contact, Howard C. Chang (changh@rowan.edu).

4.1.2. Materials availability

The *C. elegans* strains and DNA plasmids generated in this study will be shared upon request. We may require a payment to cover shipping, and a completed materials transfer agreement is required if there is potential for commercial application.

4.1.3. Data and code availability

All data reported in this paper will be shared upon request. This paper does not include any datasets that require accession numbers, DOIs, unique identifiers, or original code.

4.1.4. Strains

C. elegans strains were maintained at 20 °C using standard methods [52]. Strains were maintained at 20 °C, then shifted to 22.5 °C for *P. aeruginosa* lawn avoidance assays. The mutant strains used in this study, including *sod-1* (tm776), *fust-1* (R446S), and *fust-1*(P446L), were obtained from the Caenorhabditis Genetics Center and backcrossed six times with N2 prior to analysis. Strain of *fust-1* (tm4439) is a gift from NBRP and backcrossed six times with N2 prior to analysis. Transgenic animals KP1148 nuls25 *gr-1p*:GLR-1GFP were also obtained from the Caenorhabditis Genetics Center and backcrossed six times. Integrated transgenic animals HCX1443 bosIs1443 [*fust-1p*:FUST-1GFP; *unc-122p*:mCherry], HCX1446 bosIs1446 [*fust-1p*:FUST-1mStrawberry; *unc-122p*:GFP], HCX1536 bosIs1536 [*unc-129p*:SOD-1mScarlet; *unc-122p*:GFP], HCX1596 bosIs1557 [*eat-4p*:EAT-4GFP; *unc-122p*:mCherry], and HCX1537 bosIs1240 [*sod-1p*:rxRFP; *ges-1p*:rxRFP; *unc-122p*:GFP] were backcrossed before being crossed into *sod-1* and *fust-1* mutant strains. Because *sod-1* and *fust-1* are closely linked on chromosome II, *sod-1* (tm776); *fust-1* (tm4439) double mutants were generated using CRISPR-CAS9 by deleting the *sod-1* locus in *fust-1* (tm4439). Transgenic strains were isolated by microinjecting plasmids (typically at 100–150 µg/mL), together with one of the following co-injection markers—*unc-122p*:GFP or *unc-122p*:mCherry—in wild-type or mutant animals. UV integration of the extrachromosomal array was performed

following the protocol originated by S. Mitani [53]. The integrated lines were then backcrossed with N2 prior to analysis.

4.1.5. Antibodies and immunohistochemistry

Affinity purified FLAG-tag FUST-1 proteins were used to immunize animals to generate anti-FUST-1 polyclonal antibodies (Cocalico Biologicals). Primary polyclonal anti-FUST-1 antibodies were used at the dilution of 1:2000. Primary monoclonal anti-β-tubulin antibodies (Hybridoma Bank, E7) were used at the dilution of 1:3000. Anti-guinea pig and anti-mouse HRP-conjugated secondary antibodies were purchased from Jackson Laboratories and were used at the dilution of 1:5000. For SDS-PAGE, worms of each genotype were collected from three 100 mm × 15 mm plates. Crude lysates were treated with protease inhibitors (Roche) and 30 µg total proteins were loaded into each lane for the analysis.

4.1.6. *P. aeruginosa* avoidance assay

A 100 mL solution of LB was inoculated with a single colony of *P. aeruginosa* PA14 and grown overnight without shaking at 22.5 °C for 48 h until O.D. reached 0.2–0.3. 30 µL of this culture was used to seed the center of the 60 mm NGM plate. Seeded plates were incubated for 24 h at room temperature (22.5 °C) prior to the experiment. Approximately 30 animals (young adults) were transferred onto plates containing the *P. aeruginosa* PA14 lawn at 22.5 °C, and lawn occupancy was measured at the indicated times. Three plates of each genotype were used in each experiment, and all experiments were performed at least three times. Upon being transferred to the *P. aeruginosa*-containing plates, animals explored the plate for about 10–15 min until they found the bacterial lawn and then remained on the lawn. Subsequently, lawn occupancy was measured over time as the lawn avoidance behavior was observed [43].

4.1.7. Molecular cloning

The promoter region of *eat-4* was amplified by PCR using primers 5'-TGCTGGCGCCCCCATATCTC - 3' and 5'-GATGATGATGATGATGAGTTGTTGTAAGAGGAAGG - 3'. The cDNA of *eat-4* was synthesized based on the sequence of *eat-4* cDNA isoform a from WormBase. The *eat-4* promoter and *eat-4* cDNA were cloned using *SphI/KpnI* and *KpnI/NheI* cloning sites respectively onto a pUC57 mini vector that contains GFP. The rescue construct of *fust-1* is a transgene that contains the *fust-1* genomic sequence with either GFP or mStrawberry fusion at the carboxyl end of FUST-1. Plasmid containing rxRFP cDNA were obtained from Addgene [42]. Detailed primer sets and methods used for cloning are available upon request.

4.1.8. Microscopy

Animals were mounted in M9 with levamisole (10 mM) or with beads onto slides with a 3 % agarose pad. The slides were viewed using an AxioImager fluorescence microscope with 20x/0.5 and 40x/0.75 objectives. The fluorescence signals were recorded by a CCD camera in a 16-bit format without saturation.

4.2. Quantification and statistical analysis

The images were captured and analyzed using MetaMorph imaging software. For all experiments, the significance of differences between conditions was evaluated with GraphPad Prism software. Data sets were either analyzed using one-way ANOVA followed by Tukey's multiple comparison test or analyzed and determined by Welch's *t*-test.

Contributions

C.H.W. and A.R. performed the experiments and contributed to the draft of the manuscript. H.C.C. designed and performed the experiments, analyzed the results, and wrote the paper.

KEY RESOURCES TABLE

REAGENT or RESOURCE	SOURCE	IDENTIFIER
Bacterial and virus strains		
<i>Pseudomonas aeruginosa</i> PA14	Ausubel Lab	WB Cat# WBStrain00041978
<i>Escherichia coli</i> OP50	CGC	WB Cat# WBStrain00041969
Experimental models: Organisms/strains		
<i>C. elegans</i> : N2	CGC	WB Cat# WBStrain00000001
<i>C. elegans</i> : GA187 <i>sod-1</i> (<i>tm776</i>)	CGC	WB Cat# WBStrain00007662
<i>C. elegans</i> : HCX1407 <i>fust-1</i> (<i>R446S</i>) 6x backcross from HA2846	CGC	N/A
<i>C. elegans</i> : HCX1405 <i>fust-1</i> (<i>P447L</i>) 6x backcross from HA2847	CGC	N/A
<i>C. elegans</i> : HCX475 <i>fust-1</i> (<i>tm4439</i>) 6x backcross	NBRP	N/A
<i>C. elegans</i> : HCX1101 <i>sod-1</i> (<i>tm776</i>); <i>fust-1</i> (<i>tm4439</i>) 6x backcross	This study	N/A
<i>C. elegans</i> : HCX1443 <i>bosIs1443</i> [<i>fust-1p::FUST-1::GFP</i> ; <i>unc-122p::mCherry</i>] 4x backcross	This study	N/A
<i>C. elegans</i> : HCX1446 <i>bosIs1446</i> [<i>fust-1p::FUST-1::mStrawberry</i> ; <i>unc-122p::GFP</i>] 4x backcross	This study	N/A
<i>C. elegans</i> : HCX1536 <i>bosIs1536</i> [<i>unc-129p::SOD-1::mScarlet</i> ; <i>unc-122p::GFP</i>] 4x backcross	This study	N/A
<i>C. elegans</i> : HCX1596 <i>bosIs1557</i> [<i>eat-4p::EAT-4::GFP</i> ; <i>unc-122p::mCherry</i>] 5x backcross	This study	N/A
<i>C. elegans</i> : HCX1537 <i>bosIs1240</i> [<i>sod-1p::rxRFP</i> ; <i>ges-1p::rxRFP</i> ; <i>unc-122p::GFP</i>] 4x backcross	This study	N/A
<i>C. elegans</i> : HCX923 <i>nuls25</i> [<i>glr-1p::glr-1::GFP</i>] 4x backcross from KP1148	This study	N/A
<i>C. elegans</i> : HCX1477 <i>fust-1</i> (<i>tm4439</i>); <i>bosIs1443</i> [<i>fust-1p::FUST-1::GFP</i> ; <i>unc-122p::mCherry</i>]	This study	N/A
<i>C. elegans</i> : HCX1480 <i>fust-1</i> (<i>tm4439</i>); <i>bosIs1446</i> [<i>fust-1p::FUST-1::mStrawberry</i> ; <i>unc-122p::GFP</i>]	This study	N/A
<i>C. elegans</i> : HCX1572 <i>fust-1</i> (<i>tm4439</i>); <i>bosIs1536</i> [<i>unc-129p::SOD-1::mScarlet</i> ; <i>unc-122p::GFP</i>]	This study	N/A
<i>C. elegans</i> : HCX1575 <i>sod-1</i> (<i>tm776</i>); <i>fust-1</i> (<i>tm4439</i>); <i>bosIs1536</i> [<i>unc-129p::SOD-1::mScarlet</i> ; <i>unc-122p::GFP</i>]	This study	N/A
<i>C. elegans</i> : HCX1579 <i>fust-1</i> (<i>R446S</i>); <i>bosIs1536</i> [<i>unc-129p::SOD-1::mScarlet</i> ; <i>unc-122p::GFP</i>]	This study	N/A
<i>C. elegans</i> : HCX1581 <i>fust-1</i> (<i>P447L</i>); <i>bosIs1536</i> [<i>unc-129p::SOD-1::mScarlet</i> ; <i>unc-122p::GFP</i>]	This study	N/A
<i>C. elegans</i> : HCX1585 <i>fust-1</i> (<i>tm4439</i>); <i>bosIs1443</i> [<i>fust-1p::FUST-1::GFP</i> ; <i>unc-122p::mCherry</i>]; <i>bosIs1536</i> [<i>unc-129p::SOD-1::mScarlet</i> ; <i>unc-122p::GFP</i>]	This study	N/A
<i>C. elegans</i> : HCX1605 <i>fust-1</i> (<i>tm4439</i>); <i>bosIs1557</i> [<i>eat-4p::EAT-4::GFP</i> ; <i>unc-122p::mCherry</i>]	This study	N/A
<i>C. elegans</i> : HCX1618 <i>fust-1</i> (<i>R446S</i>); <i>bosIs1557</i> [<i>eat-4p::EAT-4::GFP</i> ; <i>unc-122p::mCherry</i>]	This study	N/A
<i>C. elegans</i> : HCX1622 <i>fust-1</i> (<i>P447L</i>); <i>bosIs1557</i> [<i>eat-4p::EAT-4::GFP</i> ; <i>unc-122p::mCherry</i>]	This study	N/A
<i>C. elegans</i> : HCX1648 <i>sod-1</i> (<i>tm776</i>); <i>bosIs1557</i> [<i>eat-4p::EAT-4::GFP</i> ; <i>unc-122p::mCherry</i>]	This study	N/A
<i>C. elegans</i> : HCX1665 <i>fust-1</i> (<i>tm4439</i>); <i>bosIs1557</i> [<i>eat-4p::EAT-4::GFP</i> ; <i>unc-122p::mCherry</i>]; <i>bosIs1446</i> [<i>fust-1p::FUST-1::mStrawberry</i> ; <i>unc-122p::GFP</i>]	This study	N/A
<i>C. elegans</i> : HCX742 <i>fust-1</i> (<i>tm4439</i>); <i>nuls25</i> [<i>glr-1p::glr-1::GFP</i>]	This study	N/A
<i>C. elegans</i> : HCX937 <i>fust-1</i> (<i>R446S</i>); <i>nuls25</i> [<i>glr-1p::glr-1::GFP</i>]	This study	N/A
<i>C. elegans</i> : HCX940 <i>fust-1</i> (<i>P447L</i>); <i>nuls25</i> [<i>glr-1p::glr-1::GFP</i>]	This study	N/A
<i>C. elegans</i> : HCX1398 <i>fust-1</i> (<i>tm4439</i>); <i>bosIs1240</i> [<i>sod-1p::rxRFP</i> ; <i>ges-1p::rxRFP</i> ; <i>unc-122p::GFP</i>]	This study	N/A
<i>C. elegans</i> : HCX1516 <i>fust-1</i> (<i>R446S</i>); <i>bosIs1240</i> [<i>sod-1p::rxRFP</i> ; <i>ges-1p::rxRFP</i> ; <i>unc-122p::GFP</i>]	This study	N/A
<i>C. elegans</i> : HCX1519 <i>fust-1</i> (<i>P447L</i>); <i>bosIs1240</i> [<i>sod-1p::rxRFP</i> ; <i>ges-1p::rxRFP</i> ; <i>unc-122p::GFP</i>]	This study	N/A
<i>C. elegans</i> : HCX1522 <i>fust-1</i> (<i>tm4439</i>); <i>bosIs1240</i> [<i>sod-1p::rxRFP</i> ; <i>ges-1p::rxRFP</i> ; <i>unc-122p::GFP</i>]; <i>bosIs1443</i> [<i>fust-1p::FUST-1::GFP</i> ; <i>unc-122p::mCherry</i>]	This study	N/A
<i>C. elegans</i> : HCX1870 <i>fust-1</i> (<i>R446S</i>); <i>bosIs1557</i> [<i>eat-4p::EAT-4::GFP</i> ; <i>unc-122p::mCherry</i>]; <i>bosIs1446</i> [<i>fust-1p::FUST-1::mStrawberry</i> ; <i>unc-122p::GFP</i>]	This study	N/A
<i>C. elegans</i> : HCX1871 <i>fust-1</i> (<i>P447L</i>); <i>bosIs1557</i> [<i>eat-4p::EAT-4::GFP</i> ; <i>unc-122p::mCherry</i>]; <i>bosIs1446</i> [<i>fust-1p::FUST-1::mStrawberry</i> ; <i>unc-122p::GFP</i>]	This study	N/A
Oligonucleotides		
eat-4 promoter PCR forward primer 5'-TGCTGGCGCCCGCCCATATCTC-3'	IDT	N/A
eat-4 promoter PCR reverse primer 5'-GATGATGATGATGATGGAGTTGTTGTAAGAGGAAGG-3'	IDT	N/A
sod-1 promoter PCR forward primer 5'-GAACACCAAACCGGACTGACCAAGT-3'	IDT	N/A
sod-1 promoter PCR reverse primer 5'-CAAAGTTGTAGATTCAGTATTTTATAGATCGGTG-3'	IDT	N/A
unc-129 promoter PCR forward primer 5'-CATGTCTTTTACCTCTTTTGGCATGTACCGTTCTTC-3'	IDT	N/A
unc-129 promoter PCR reverse primer 5'-GGATCAAACAAATAAGATGCGGAGTTCTCAAATAG-3'	IDT	N/A
Recombinant DNA		
pUC57 mini GFP	This study	N/A
pUC57 mini mScarlet	This study	N/A
pUC57 simple eat-4 cDNA	This study	N/A
pUC57 simple rxRFP cDNA	This study	N/A
Software and algorithms		
GraphPad Prism 9.0	GraphPad Prism Software, Inc	https://www.graphpad.com/
MetaMorph	Molecular Devices	https://www.moleculardevices.com/

Declaration of competing interest

The authors declare that they have no known competing financial interests or personal relationships that could have appeared to influence the work reported in this paper

Acknowledgments

We thank the Caenorhabditis Genetics Center (CGC), which is supported by the NIH grant P40 OD010440, for providing us with many strains. We thank National Bioresource Project (NBRP) in Japan for strains. This work was supported by the NIH grant R01 GM131156 to H. C.C.

Appendix A. Supplementary data

Supplementary data to this article can be found online at <https://doi.org/10.1016/j.freeradbiomed.2023.11.015>.

References

- [1] O. Hardiman, et al., Amyotrophic lateral sclerosis, *Nat. Rev. Dis. Prim.* 3 (2017), 17071, <https://doi.org/10.1038/nrdp.2017.71>.
- [2] R. Mejzini, et al., ALS genetics, mechanisms, and therapeutics: where are we now? *Front. Neurosci.* 13 (2019) 1310, <https://doi.org/10.3389/fnins.2019.01310>.
- [3] E.T. Cirulli, et al., Exome sequencing in amyotrophic lateral sclerosis identifies risk genes and pathways, *Science* 347 (2015) 1436–1441, <https://doi.org/10.1126/science.aaa3650>.
- [4] A. Freischmidt, et al., Haploinsufficiency of TBK1 causes familial ALS and frontotemporal dementia, *Nat. Neurosci.* 18 (2015) 631–636, <https://doi.org/10.1038/nn.4000>.
- [5] T.J. Kwiatkowski Jr., et al., Mutations in the FUS/TLS gene on chromosome 16 cause familial amyotrophic lateral sclerosis, *Science* 323 (2009) 1205–1208, <https://doi.org/10.1126/science.1166066>.
- [6] D.R. Rosen, et al., Mutations in Cu/Zn superoxide dismutase gene are associated with familial amyotrophic lateral sclerosis, *Nature* 362 (1993) 59–62, <https://doi.org/10.1038/362059a0>.
- [7] J. Sreedharan, et al., TDP-43 mutations in familial and sporadic amyotrophic lateral sclerosis, *Science* 319 (2008) 1668–1672, <https://doi.org/10.1126/science.1154584>.
- [8] G.G. Hicks, et al., Fus deficiency in mice results in defective B-lymphocyte development and activation, high levels of chromosomal instability and perinatal death, *Nat. Genet.* 24 (2000) 175–179, <https://doi.org/10.1038/72842>.
- [9] S.L. Huang, et al., A robust TDP-43 knock-in mouse model of ALS, *Acta Neuropathol Commun* 8 (2020) 3, <https://doi.org/10.1186/s40478-020-0881-5>.
- [10] J. Lopez-Erauskin, et al., ALS/FTD-Linked mutation in FUS suppresses intra-axonal protein synthesis and drives disease without nuclear loss-of-function of FUS, *Neuron* 100 (2018) 816–830 e817, <https://doi.org/10.1016/j.neuron.2018.09.044>.
- [11] C. Vance, et al., Mutations in FUS, an RNA processing protein, cause familial amyotrophic lateral sclerosis type 6, *Science* 323 (2009) 1208–1211, <https://doi.org/10.1126/science.1165942>.
- [12] L.I. Bruijn, et al., ALS-linked SOD1 mutant G85R mediates damage to astrocytes and promotes rapidly progressive disease with SOD1-containing inclusions, *Neuron* 18 (1997) 327–338.
- [13] L.I. Bruijn, et al., Aggregation and motor neuron toxicity of an ALS-linked SOD1 mutant independent from wild-type SOD1, *Science* 281 (1998) 1851–1854.
- [14] S.C. Ling, et al., Overriding FUS autoregulation in mice triggers gain-of-toxic dysfunctions in RNA metabolism and autophagy-lysosome axis, *Elife* 8 (2019), <https://doi.org/10.7554/eLife.40811>.
- [15] G. Kim, O. Gautier, E. Tassoni-Tsichida, X.R. Ma, A.D. Gitler, ALS genetics: gains, losses, and implications for future therapies, *Neuron* 108 (2020) 822–842, <https://doi.org/10.1016/j.neuron.2020.08.022>.
- [16] K. Forsberg, et al., Misfolded SOD1 inclusions in patients with mutations in C9orf72 and other ALS/FTD-associated genes, *J. Neurol. Neurosurg. Psychiatry* 90 (2019) 861–869, <https://doi.org/10.1136/jnnp-2018-319386>.
- [17] Y. Kokubo, et al., Accumulation of neurofilaments and SOD1-immunoreactive products in a patient with familial amyotrophic lateral sclerosis with I113T SOD1 mutation, *Arch. Neurol.* 56 (1999) 1506–1508, <https://doi.org/10.1001/archneur.56.12.1506>.
- [18] F.L. Muller, et al., Absence of CuZn superoxide dismutase leads to elevated oxidative stress and acceleration of age-dependent skeletal muscle atrophy, *Free Radic. Biol. Med.* 40 (2006) 1993–2004, <https://doi.org/10.1016/j.freeradbiomed.2006.01.036>.
- [19] T. Oeda, et al., Oxidative stress causes abnormal accumulation of familial amyotrophic lateral sclerosis-related mutant SOD1 in transgenic *Caenorhabditis elegans*, *Hum. Mol. Genet.* 10 (2001) 2013–2023.
- [20] J.S. Valentine, P.A. Doucette, S. Zittin Potter, Copper-zinc superoxide dismutase and amyotrophic lateral sclerosis, *Annu. Rev. Biochem.* 74 (2005) 563–593, <https://doi.org/10.1146/annurev.biochem.74.121801.161647>.
- [21] A. Al-Chalabi, et al., Stage of prolonged survival in ALS - author's reply, *Lancet Neurol.* 17 (2018) 579–580, [https://doi.org/10.1016/S1474-4422\(18\)30208-4](https://doi.org/10.1016/S1474-4422(18)30208-4).
- [22] G. Bensimon, L. Lacomblez, V. Meininger, A controlled trial of riluzole in amyotrophic lateral sclerosis. ALS/Riluzole Study Group, *N. Engl. J. Med.* 330 (1994) 585–591, <https://doi.org/10.1056/NEJM199403033300901>.
- [23] A. Platakis, E. Constantakakis, J. Smith, The neuroexcitotoxic amino acids glutamate and aspartate are altered in the spinal cord and brain in amyotrophic lateral sclerosis, *Ann. Neurol.* 24 (1988) 446–449, <https://doi.org/10.1002/ana.410240314>.
- [24] J.D. Rothstein, et al., Abnormal excitatory amino acid metabolism in amyotrophic lateral sclerosis, *Ann. Neurol.* 28 (1990) 18–25, <https://doi.org/10.1002/ana.410280106>.
- [25] R.Y. Lee, E.R. Sawin, M. Chalfie, H.R. Horvitz, L. Avery, EAT-4, a homolog of a mammalian sodium-dependent inorganic phosphate cotransporter, is necessary for glutamatergic neurotransmission in *Caenorhabditis elegans*, *J. Neurosci.* 19 (1999) 159–167, <https://doi.org/10.1523/JNEUROSCI.19-01-00159.1999>.
- [26] E. Serrano-Saiz, et al., SLC17A6/7/8 vesicular glutamate transporter homologs in nematodes, *Genetics* 214 (2020) 163–178, <https://doi.org/10.1534/genetics.119.302855>.
- [27] P.J. Brockie, D.M. Madsen, Y. Zheng, J. Mellem, A.V. Maricq, Differential expression of glutamate receptor subunits in the nervous system of *Caenorhabditis elegans* and their regulation by the homeodomain protein UNC-42, *J. Neurosci.* 21 (2001) 1510–1522, <https://doi.org/10.1523/JNEUROSCI.21-05-01510.2001>.
- [28] H.C. Chang, C. Rongo, Cytosolic tail sequences and subunit interactions are critical for synaptic localization of glutamate receptors, *J. Cell Sci.* 118 (2005) 1945–1956, <https://doi.org/10.1242/jcs.02320>.
- [29] S.C. Barber, P.J. Shaw, Oxidative stress in ALS: key role in motor neuron injury and therapeutic target, *Free Radic. Biol. Med.* 48 (2010) 629–641, <https://doi.org/10.1016/j.freeradbiomed.2009.11.018>.
- [30] A.M. Horspool, H.C. Chang, Superoxide dismutase SOD-1 modulates *C. elegans* pathogen avoidance behavior, *Sci. Rep.* 7 (2017), 45128, <https://doi.org/10.1038/srep45128>.
- [31] A.M. Horspool, H.C. Chang, Neuron-specific regulation of superoxide dismutase amid pathogen-induced gut dysbiosis, *Redox Biol.* 17 (2018) 377–385, <https://doi.org/10.1016/j.redox.2018.05.007>.
- [32] C.Y. Yu, H.C. Chang, Glutamate signaling mediates *C. elegans* behavioral plasticity to pathogens, *iScience* 25 (2022), 103919, <https://doi.org/10.1016/j.isci.2022.103919>.
- [33] S.N. Baskoylu, et al., Disrupted autophagy and neuronal dysfunction in *C. elegans* knockin models of FUS amyotrophic lateral sclerosis, *Cell Rep.* 38 (2022), 110195, <https://doi.org/10.1016/j.celrep.2021.110195>.
- [34] D. Dormann, et al., Arginine methylation next to the PY-NLS modulates Transportin binding and nuclear import of FUS, *EMBO J.* 31 (2012) 4258–4275, <https://doi.org/10.1038/emboj.2012.261>.
- [35] D. Dormann, et al., ALS-associated fused in sarcoma (FUS) mutations disrupt Transportin-mediated nuclear import, *EMBO J.* 29 (2010) 2841–2857, <https://doi.org/10.1038/emboj.2010.143>.
- [36] T. Murakami, et al., ALS/FTD mutation-induced phase transition of FUS liquid droplets and reversible hydrogels into irreversible hydrogels impairs RNP granule function, *Neuron* 88 (2015) 678–690, <https://doi.org/10.1016/j.neuron.2015.10.030>.
- [37] T. Murakami, et al., ALS mutations in FUS cause neuronal dysfunction and death in *Caenorhabditis elegans* by a dominant gain-of-function mechanism, *Hum. Mol. Genet.* 21 (2012) 1–9, <https://doi.org/10.1093/hmg/ddr417>.
- [38] R.R. Sama, et al., FUS/TLS assembles into stress granules and is a prosurvival factor during hyperosmolar stress, *J. Cell. Physiol.* 228 (2013) 2222–2231, <https://doi.org/10.1002/jcp.24395>.
- [39] A.C. Hart, S. Sims, J.M. Kaplan, Synaptic code for sensory modalities revealed by *C. elegans* GLR-1 glutamate receptor, *Nature* 378 (1995) 82–85, <https://doi.org/10.1038/378082a0>.
- [40] A.V. Maricq, E. Peckol, M. Driscoll, C.I. Bargmann, Mechanosensory signalling in *C. elegans* mediated by the GLR-1 glutamate receptor, *Nature* 378 (1995) 78–81, <https://doi.org/10.1038/378078a0>.
- [41] C. Rongo, C.W. Whitfield, A. Rodal, S.K. Kim, J.M. Kaplan, LIN-10 is a shared component of the polarized protein localization pathways in neurons and epithelia, *Cell* 94 (1998) 751–759, [https://doi.org/10.1016/S0092-8674\(00\)81734-1](https://doi.org/10.1016/S0092-8674(00)81734-1).
- [42] Y. Fan, Z. Chen, H.W. Ai, Monitoring redox dynamics in living cells with a redox-sensitive red fluorescent protein, *Anal. Chem.* 87 (2015) 2802–2810, <https://doi.org/10.1021/ac5041988>.
- [43] H.C. Chang, J. Paek, D.H. Kim, Natural polymorphisms in *C. elegans* HECW-1 E3 ligase affect pathogen avoidance behaviour, *Nature* 480 (2011) 525–529, <https://doi.org/10.1038/nature10643>.
- [44] T.M. Miller, et al., Trial of antisense oligonucleotide tofersen for SOD1 ALS, *N. Engl. J. Med.* 387 (2022) 1099–1110, <https://doi.org/10.1056/NEJMoa2204705>.
- [45] S. Paganoni, et al., Trial of sodium phenylbutyrate-taurursodiol for amyotrophic lateral sclerosis, *N. Engl. J. Med.* 383 (2020) 919–930, <https://doi.org/10.1056/NEJMoa1916945>.
- [46] S. Witzel, et al., Safety and effectiveness of long-term intravenous administration of edaravone for treatment of patients with amyotrophic lateral sclerosis, *JAMA Neurol.* 79 (2022) 121–130, <https://doi.org/10.1001/jamaneuro.2021.4893>.
- [47] D.J. Dickinson, J.D. Ward, D.J. Reiner, B. Goldstein, Engineering the *Caenorhabditis elegans* genome using Cas9-triggered homologous recombination, *Nat. Methods* 10 (2013) 1028–1034, <https://doi.org/10.1038/nmeth.2641>.
- [48] A.E. Friedland, et al., Heritable genome editing in *C. elegans* via a CRISPR-Cas9 system, *Nat. Methods* 10 (2013) 741–743, <https://doi.org/10.1038/nmeth.2532>.
- [49] H. Kim, et al., A co-CRISPR strategy for efficient genome editing in *Caenorhabditis elegans*, *Genetics* 197 (2014) 1069–1080, <https://doi.org/10.1534/genetics.114.166389>.
- [50] S.G. Carriedo, S.L. Sensi, H.Z. Yin, J.H. Weiss, AMPA exposures induce mitochondrial Ca(2+) overload and ROS generation in spinal motor neurons in vitro, *J. Neurosci.* 20 (2000) 240–250, <https://doi.org/10.1523/JNEUROSCI.20-01-00240.2000>.
- [51] R. Sattler, M. Tymianski, Molecular mechanisms of glutamate receptor-mediated excitotoxic neuronal cell death, *Mol. Neurobiol.* 24 (2001) 107–129, <https://doi.org/10.1385/MN:24:1-3:107>.
- [52] S. Brenner, The genetics of *Caenorhabditis elegans*, *Genetics* 77 (1974) 71–94.
- [53] E. Kage-Nakadai, R. Imae, S. Yoshina, S. Mitani, Methods for single/low-copy integration by ultraviolet and trimethylpsoralen treatment in *Caenorhabditis elegans*, *Methods* 68 (2014) 397–402, <https://doi.org/10.1016/j.ymeth.2014.02.036>.